Molecular Imaging of Fibroblast Activity After Myocardial Infarction Using a ^{68}Ga-Labeled Fibroblast Activation Protein Inhibitor, FAPI-04

Zohreh Varasteh[1], Sarajo Mohanta[2,3], Stephanie Robu[1], Miriam Braeuer[1], Yuanfang Li[2], Negar Omidvari[1], Geoffrey Topping[1], Ting Sun[2], Stephan G. Nekolla[1], Antonia Richter[1], Christian Weber[2,3], Andreas Habenicht[2], Uwe A. Haberkorn[4], and Wolfgang A. Weber[1]

[1]Department of Nuclear Medicine, Klinikum rechts der Isar der TUM, Munich, Germany; [2]Institute for Cardiovascular Prevention, Ludwig-Maximilians-Universität, Munich, Germany; [3]German Centre for Cardiovascular Research, Munich Heart Alliance, Munich, Germany; and [4]Department of Nuclear Medicine, University of Heidelberg, Heidelberg, Germany

Heart failure remains a major source of late morbidity and mortality after myocardial infarction (MI). The temporospatial presence of activated fibroblasts in the injured myocardium predicts the quality of cardiac remodeling after MI. Therefore, monitoring of activated fibroblasts is of great interest for studying cardiac remodeling after MI. Fibroblast activation protein (FAP) expression is upregulated in activated fibroblasts. This study investigated the feasibility of imaging activated fibroblasts with a new ^{68}Ga-labeled FAP inhibitor (^{68}Ga-FAPI-04) for PET imaging of fibroblast activation in a preclinical model of MI. **Methods:** MI and sham-operated rats were scanned with ^{68}Ga-FAPI-04 PET/CT (1, 3, 6, 14, 23, and 30 d after MI) and with ^{18}F-FDG (3 d after MI). Dynamic ^{68}Ga-FAPI-04 PET and blocking studies were performed on MI rats 7 d after coronary ligation. After in vivo scans, the animals were euthanized and their hearts harvested for ex vivo analyses. Cryosections were prepared for autoradiography, hematoxylin and eosin (H&E), and immunofluorescence staining. **Results:** ^{68}Ga-FAPI-04 uptake in the injured myocardium peaked on day 6 after coronary ligation. The tracer accumulated intensely in the MI territory, as identified by decreased ^{18}F-FDG uptake and confirmed by PET/MR and H&E staining. Autoradiography and H&E staining of cross-sections revealed that ^{68}Ga-FAPI-04 accumulated mainly at the border zone of the infarcted myocardium. In contrast, there was only minimal uptake in the infarct of the blocked rats, comparable to the uptake in the remote noninfarcted myocardium (PET image–derived ratio of infarct uptake to remote uptake: 6 ± 2). Immunofluorescence staining confirmed the presence of FAP-positive myofibroblasts in the injured myocardium. Morphometric analysis of the whole-heart sections demonstrated 3- and 8-fold higher FAP-positive fibroblast density in the border zone than in the infarct center and remote area, respectively. **Conclusion:** ^{68}Ga-FAPI-04 represents a promising radiotracer for in vivo imaging of post-MI fibroblast activation. Noninvasive imaging of activated fibroblasts may have significant diagnostic and prognostic value, which could aid clinical management of patients after MI.

Key Words: myocardial infarction; cardiac remodeling; fibroblast activation protein; molecular imaging; PET

J Nucl Med 2019; 60:1743–1749
DOI: 10.2967/jnumed.119.226993

Cardiac remodeling is a key factor for the prognosis of patients who survive a myocardial infarction (MI) (*1*). Adverse cardiac remodeling can lead to heart failure, which is a major cause of morbidity and mortality worldwide (*2*). After MI, fibrotic response plays a critical role in left ventricular remodeling (*3*). Activated cardiac fibroblasts have been identified as central mediators of this reparative response (*4*).

After MI, fibroblasts undergo dynamic phenotypic changes and differentiate into collagen-secreting proto-myofibroblasts. These activated fibroblasts can further differentiate into mature myofibroblasts. After MI, activated fibroblasts migrate into the injured myocardium and contribute to tissue replacement, thereby helping to preserve the structural integrity of the infarcted heart. They secrete increased amounts of cytokines, growth factors, and pericellular proteases to maintain the extracellular matrix (ECM) and promote replacement fibrosis—formation of a scar that stabilizes the ventricular wall and maintains the macroanatomy of the heart. Although the initial replacement and reparative fibrosis are pivotal for the prevention of ventricular wall rupture after an ischemic insult, they also induce geometric, biomechanical, and biochemical changes in areas remote from the infarction and elicit reactive and interstitial fibrosis. Excessive fibrosis and persistence of active fibroblasts within the myocardium can lead to increased left ventricular stiffness and hence decreased cardiac contraction. Furthermore, the presence of excessive ECM may decrease oxygen and nutrient availability to the myocardium, contributing to detrimental cardiac remodeling. Noninvasive imaging of activated fibroblasts could therefore provide unique opportunities to study cardiac remodeling over time and to monitor therapeutic interventions that aim to prevent a progressive decline of ventricular function (*5,6*).

Fibroblast activation protein (FAP) is a homodimeric membrane-bound serine protease that has intracellular and extracellular soluble truncated forms. FAP is specifically expressed by activated fibroblasts during wound healing (*7*). Elevated expression of FAP in

Received Feb. 1, 2019; revision accepted May 29, 2019.
For correspondence or reprints contact: Zohreh Varasteh, Department of Nuclear Medicine, Klinikum rechts der Isar der TUM, Ismaningerstrasse 22, 81675 Munich, Germany.
E-mail: zohreh.varasteh@tum.de
Published online Aug. 12, 2019.

myofibroblasts has been reported in rat hearts with permanent MI and in the hearts of patients with acute MI (*8*). Recently, radiolabeled FAP inhibitors (FAPIs) for noninvasive imaging of FAP expression have been developed and characterized by Haberkorn's group (*9,10*). PET imaging with radiolabeled FAPIs has shown desirable biodistribution and high uptake by activated stromal fibroblasts in murine experimental tumors, as well as in patients with different malignancies (*9,10*). In the present study, our objective was to evaluate the feasibility of imaging activated fibroblasts after MI using a ^{68}Ga-labeled FAPI (^{68}Ga-FAPI-04).

MATERIALS AND METHODS

Experimental MI in Rats

Twenty Wistar rats (male, 3 mo old, 340−365 g; Charles River) were subjected to MI by permanent ligation of the left anterior descending coronary artery. The animals were anesthetized by intramuscular administration of a 0.5 mg/kg dose of medetomidine (Pfizer), a 5 mg/kg dose of midazolam (Roche), and a 0.05 mg/kg dose of fentanyl (Ratiopharm) and artificially ventilated using a rodent ventilator for thoracotomy and permanent ligation of the left coronary artery with a 7-0 polypropylene suture. Successful coronary occlusions were verified visually by identification of cyanosis or paling of the myocardium downstream from the suture. Sham-operated animals (n = 4) underwent the same surgical procedure except the ligation. The experiments were approved by the local animal care committee and were in accordance with the German Animal Welfare Act (Regierung von Oberbayern).

Radiolabeling

^{68}Ga-labeling of FAPI-04 was performed using a fully automated, good-manufacturing-practice–compliant procedure in a GallElut^{+} synthesis module (Scintomics). A ^{68}Ge/^{68}Ga generator (iThemba Labs) was eluted with 1.0 M aqueous HCl, and a 1.2-mL fraction containing the highest activity (~500−600 MBq) was transferred into a reactor vial containing 20 nmol of FAPI-04 in 900 μL of 2.7 M 4-(2-hydroxyethyl)-1-piperazineethanesulfonic acid to adjust the pH of the reaction mixture to 3.5. While the mixture was heated at 95°C for 5 min, air was slowly bubbled through the solution for agitation. For purification, the reaction mixture was passed through a C18 Sep-Pak Light solid-phase extraction cartridge (Waters), which was preconditioned by purging with ethanol (5 mL) and water (10 mL). The cartridge was rinsed with 10 mL of water, and ^{68}Ga-FAPI-04 was eluted from the cartridge with 2 mL of ethanol/water (1/1, v/v), followed by purging with 1 mL of phosphate-buffered saline (pH 7.4) and 1 mL of water. For in vivo studies, ethanol was evaporated to exhibit the appropriate pH and osmolality for injection. Quality control of ^{68}Ga-FAPI-04 was performed using radio–reverse-phase high-performance liquid chromatography and radio–thin-layer chromatography.

In Vivo (PET/CT) Imaging

Scans were acquired on a small-animal Inveon PET/CT scanner (Siemens). Static PET/CT images were acquired 1 h after injection of ^{68}Ga-FAPI-04 (20−25 MBq; 4 nmol; 1, 3, 6, 14, 23, and 30 d after MI) and ^{18}F-FDG (8−10 MBq; 3 d after MI), with an acquisition time of 20 min. Images were reconstructed using Siemens Inveon software, which uses a 3-dimensional ordered-subsets expectation maximum algorithm with attenuation correction. Dynamic PET scans were acquired with ^{68}Ga-FAPI-04 (7 d after MI) for 90 min. Acquired data were then Fourier-rebinned in 46 time frames (6 × 5 s, 21 × 10 s, 8 × 120 s, 8 × 300 s, and 3 × 600 s) and reconstructed using the same 3-dimensional ordered-subsets expectation maximum algorithm. For quantification of tracer uptake, circular 2-dimensional regions of interest were placed on axial PET/CT images of the hearts, and signal intensities were recorded as percentage injected dose per gram of tissue (%ID/g). Regions of interest were drawn corresponding to the infarcted region and a region of noninfarcted remote myocardium in the inferior septum.

Ex Vivo (PET/MR) Imaging

To validate the results obtained by in vivo PET/CT imaging and to confirm the origin of the in vivo signal, 1 heart was also scanned ex vivo. On day 7 after MI, a rat was injected with 60 MBq of ^{68}Ga-FAPI-04 and killed 1 h afterward. The heart was excised and scanned using a small-animal PET insert (MADPET4) for a 7-T MRI scanner (MR901 magnet [Agilent/GE Healthcare] with Avance III HD electronics [Bruker]) and an acquisition time of 20 min. Anatomic MR images were acquired with a 3-dimensional spoiled gradient recalled echo (fast low-angle shot) sequence. To keep the left ventricle open, the heart was filled with alginate impression material (Zitzmann). The same animal had been scanned in vivo on day 6 after MI with ^{68}Ga-FAPI-04 PET/CT.

Competition Experiment

To assess the specificity of ^{68}Ga-FAPI-04 accumulation and to confirm that uptake of ^{68}Ga-FAPI-04 in the injured myocardium was due to saturable binding to FAP, a group of MI rats (n = 3), referred to as the blocked group, was coinjected with a blocking dose (550 nmol) of nonlabeled FAPI-04 to block specific binding sites 7 d after coronary ligation. The rats underwent PET/CT imaging followed by autoradiography. The same animals had been scanned 1 d earlier (day 6 after MI) with ^{68}Ga-FAPI-04 PET/CT without injection of the blocking compound.

Autoradiography and Histology

On day 7 after MI, rats (3 MI nonblocked, 3 MI blocked, and 2 sham) were injected with ^{68}Ga-FAPI-04 and killed 1 h afterward. Serial short-axis cryosections 10 μm thick were prepared from isolated hearts. Consecutive sections were used for autoradiography and hematoxylin and eosin (H&E) staining. The ex vivo spatial distribution of radioactivity in the heart cross-sections was examined using autoradiography. H&E staining was used to determine the location and extent of areas of infarction.

Immunofluorescence Staining and Quantification of FAP-Positive (FAP^{+}) Area

Cryosections were prepared from fresh-frozen MI hearts (7 d after MI), liver, lung, skin, and healthy hearts. Tissue sections were stained with antibodies against FAP (R&D Systems) as a marker of activated fibroblasts, prolyl-4-hydroxylase β (Origene) as a marker of activated and collagen-synthesizing fibroblasts, α-smooth muscle actin (Merck) as a marker of differentiated mature myofibroblasts, and vimentin (Merck) as a general fibroblast marker, as described previously (*8*). Stained sections were imaged using an SP8 confocal laser scanning microscope and a DM6000 fluorescence microscope (Leica). For imaging of the entire surface of heart specimens, single-plane automated tile scans were acquired using a DM6 B Thunder Imager 3D Tissue (Leica) with a field of view of 5.5 × 5.5 mm, processed with Thunder software (Leica) and mosaic-merged with 20% overlaps. For morphometry of FAP^{+} area in MI hearts, 3−5 parallel sections adjacent to H&E-stained images were selected. H&E images were used to define the infarct center, border, and remote area. FAP^{+} areas were quantified within the selected areas using Image J (National Institutes of Health). Image processing included changes in brightness, contrast, and tonal range and was applied equally across the entire image.

The experimental timeline of the in vivo and ex vivo studies is illustrated in Figure 1.

Statistics

Data are expressed as mean ± SD. The Mann–Whitney U test was used to compare 2 variables, and 1-way ANOVA was used to compare

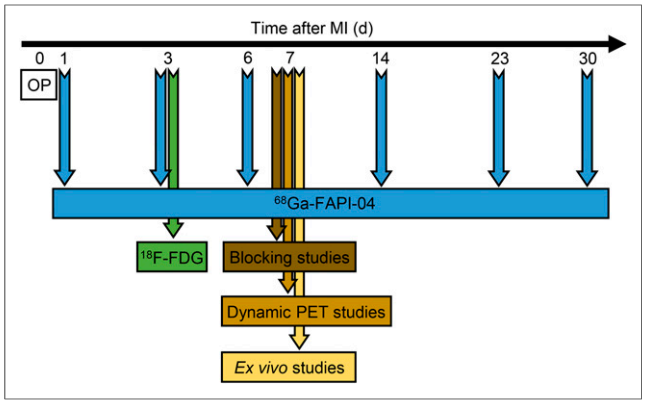

FIGURE 1. Experimental timeline. OP = operation.

multiple variables. A P value of 0.05 or less was considered to be significant. Statistical analysis was performed using SPSS Statistics software (version 24.0.0; IBM).

RESULTS

FAPI-04 was labeled with ^{68}Ga with an overall radiochemical yield of 89% ± 0.8% and radiochemical purity of at least 95%. The specific activity was 25−30 GBq/μmol.

Rapid Biodistribution and Accumulation of ^{68}Ga-FAPI-04 in MI Heart

Figure 2A shows a series of dynamic images (axial and coronal sections) from 5 to 90 min after injection of ^{68}Ga-FAPI-04 in MI heart (7 d after MI). The images demonstrate rapid clearance of ^{68}Ga-FAPI-04 from circulation via renal excretion (Supplemental Fig. 1; supplemental materials are available at http://jnm.snmjournals.org). Corresponding time–activity curves (average of 3 scans) for infarcts and noninfarct remote areas show that the tracer cleared gradually from infarcts and more rapidly from nontarget remote tissue (Fig. 2B), resulting in increasing infarct-to-noninfarct tissue ratios over time (Fig. 2C).

Specific Uptake of ^{68}Ga-FAPI-04 in Infarcts

In vivo longitudinal PET/CT images (axial sections) of a representative rat subjected to coronary ligation are shown in Figure 3A.

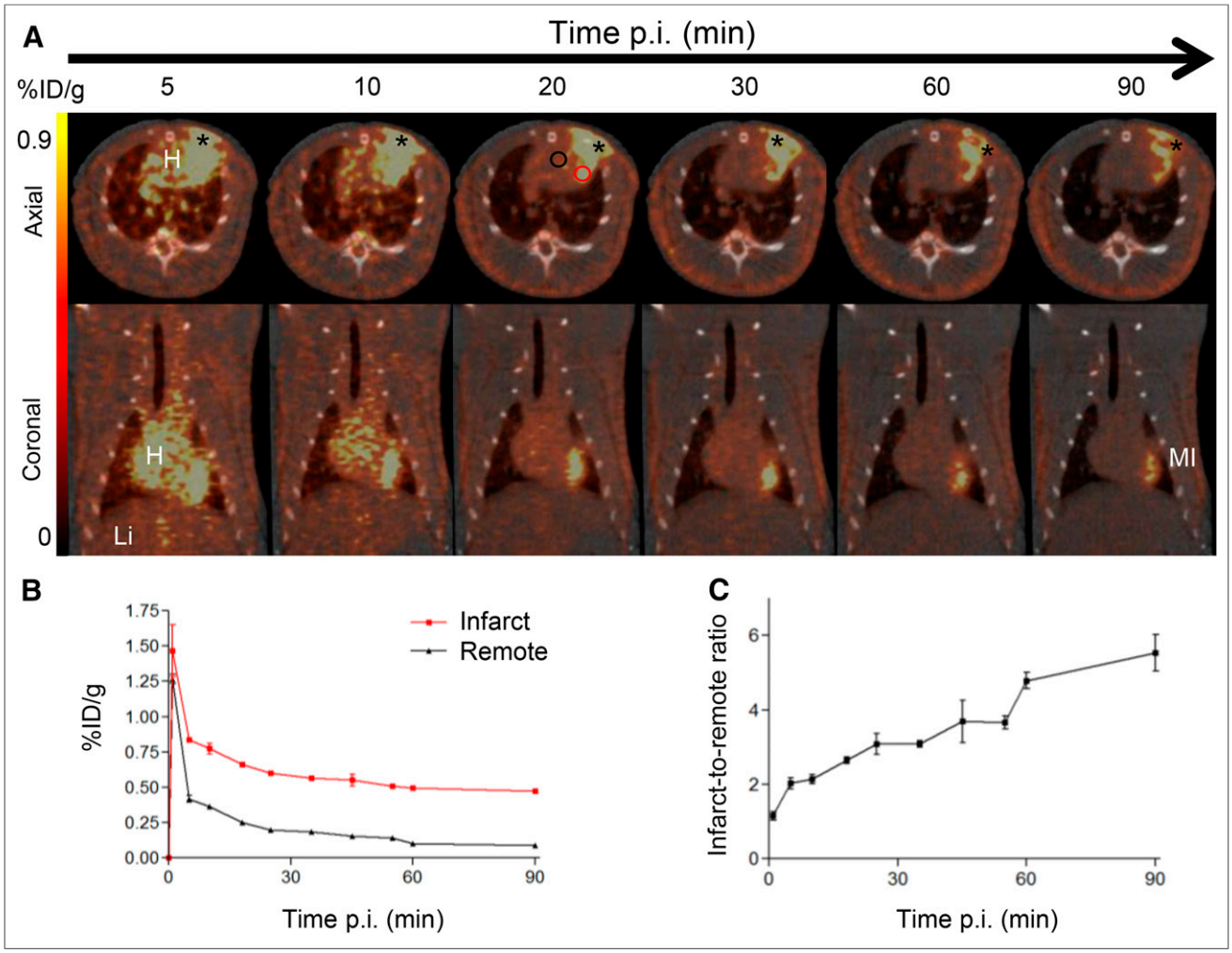

FIGURE 2. In vivo dynamic imaging of ^{68}Ga-FAPI-04 uptake. (A) Serial PET/CT images (axial and coronal sections) from 90-min dynamic scan of MI rat at 7 d after coronary ligation. Representative regions of interest (2-dimensional) drawn over infarct border zone and remote myocardium are illustrated as red and black circles, respectively. Regions of interest in infarcts were placed relatively far from surgical wounds. ^{68}Ga-FAPI-04 exhibited elevated uptake in scars from operation (asterisk). (B) Corresponding time–activity curves for infarcted and noninfarcted heart tissue (average and SD, n = 3). (C) Infarct-to-noninfarct ratio over time (average and SD, n = 3). H = heart; Li = liver; p.i. = after injection.

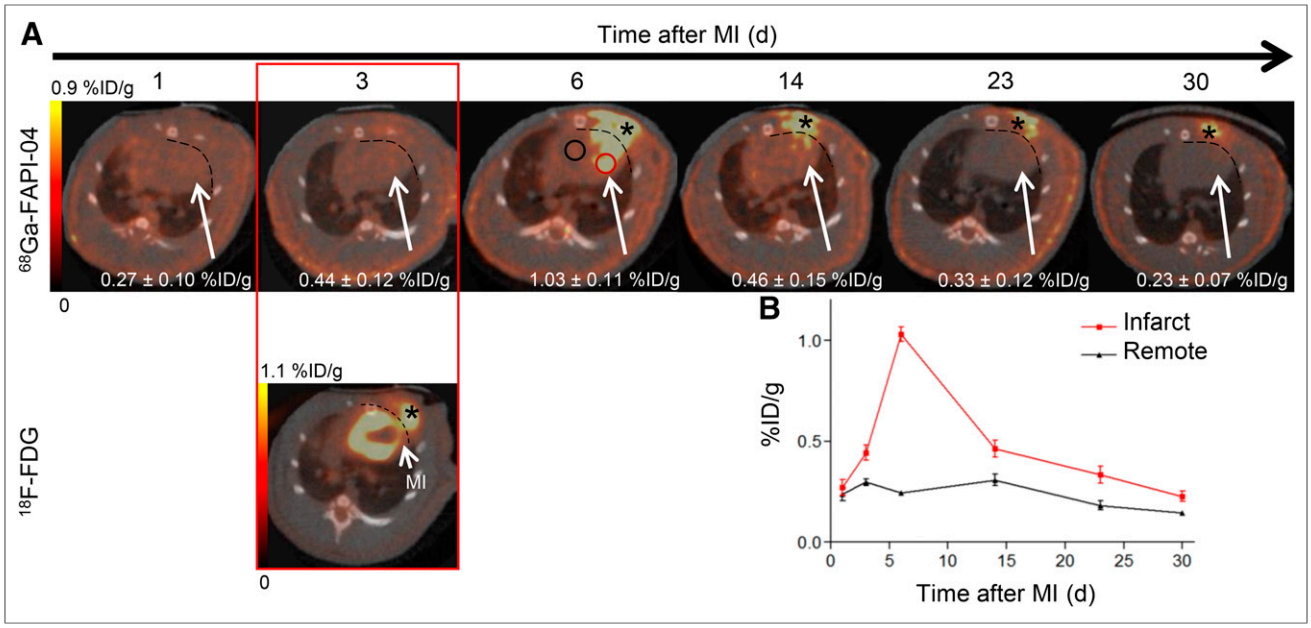

FIGURE 3. In vivo imaging of ^{68}Ga-FAPI-04 uptake in longitudinal study. (A) Static PET/CT matched axial slices in same rat subjected to coronary ligation and scanned 1 h after injection of ^{68}Ga-FAPI-04 (1, 3, 6, 14, 23, and 30 d after MI) and ^{18}F-FDG (3 d after MI). Dashed lines separate tracer uptake in myocardium from uptake in surgical wounds. In 6 d after MI image, representative regions of interest (2-dimensional) drawn over infarct border zone and remote myocardium are illustrated as red and black circles, respectively. ^{68}Ga-FAPI-04 uptake in regions of interest of infarcts is demonstrated. (B) Corresponding time–activity curves for infarcted and noninfarcted heart tissue (average and SD, $n = 3$). ^{68}Ga-FAPI-04 and ^{18}F-FDG exhibited elevated uptake in scars from operation (asterisk).

The study was performed to assess the temporal presence of activated fibroblasts in the injured myocardium.^{68}Ga-FAPI-04 uptake in the infarcts peaked on day 6 after MI (Fig. 3B). Intense ^{68}Ga-FAPI-04 uptake (1.0 ± 0.2 %ID/g) was observed in the hypometabolic MI territories that were identified on the ^{18}F-FDG PET/CT scans. Additionally, an ex vivo 7-T PET/MR scan of the heart of 1 rat was performed to better localize the ^{68}Ga-FAPI-04 signal within the intact myocardium (Fig. 4). Fusion of PET and high-resolution MR confirmed that ^{68}Ga-FAPI-04 accumulated within the infarcted myocardial region. The in vivo PET image–derived ratio of uptake in the infarct to uptake in remote myocardium was 6 ± 2 at 6 d after MI (Fig. 5B). Uptake ratios relative to other organs were also high and are summarized in Supplemental Table 1. Thus, the infarcted myocardium was imaged with high contrast 6 d after coronary ligation. The saturation of FAP by coinjection of nonlabeled FAPI-04 decreased the ^{68}Ga-FAPI-04 signal dramatically in the infarct region (0.21 ± 0.08 %ID/g, $P = 0.01$), to the same level as in the sham-operated rats (0.23 ± 0.06 %ID/g). Similarly, coinjection of nonlabeled FAPI-04 also decreased uptake of ^{68}Ga-FAPI-04 within the surgical wound, to the background level (Fig. 5A). The exact location of ^{68}Ga-FAPI-04 uptake within the myocardium was further analyzed by autoradiography and correlated with histologic findings. In autoradiography images, increased uptake of ^{68}Ga-FAPI-04 was observed predominantly in the periinfarct border zone (Fig. 6). No significant tracer uptake was observed in remote uninvolved myocardial regions or in the myocardium of sham-operated rats (Fig. 5A). The infarct-to-noninfarct signal intensity ratio was 14.1 ± 0.8 (Fig. 5C). Blocking of the binding sites with an excess of nonlabeled FAPI-04 decreased the ratio 10-fold, to 1.4 ± 0.2 ($P = 0.02$).

FAP Expression by Activated Fibroblasts in Periinfarcted Myocardium

To determine FAP expression in the myocardial connective tissue, multicolor immunofluorescence staining analyses were performed on infarcted rat hearts at 7 d after MI. Thunder Imager scans of the whole-heart slices revealed that FAP$^+$ cells selectively accumulated in the periinfarcted area rather than in the infarct center or remote healthy myocardium (Fig. 7A). Within the infarcted hearts, a few FAP$^+$ fibroblasts were located in the necrotic or fibrotic infarct area, but FAP$^+$ fibroblasts were rarely detected in the remote myocardium (Fig. 7A; Supplemental Fig. 2) or in the myocardium of healthy hearts (Supplemental Fig. 3). Enumeration of FAP$^+$ cells in MI hearts revealed 3- and 8-fold higher FAP$^+$ fibroblast density in the border zones than in the infarct center and remote areas, respectively (Fig. 7B).

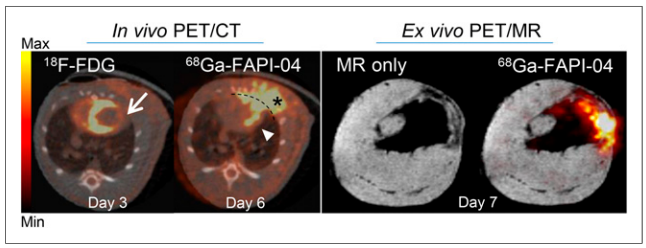

FIGURE 4. Axial sections of in vivo PET/CT imaging with ^{18}F-FDG (day 3 after MI) and ^{68}Ga-FAPI-04 (day 6 after MI) and corresponding ex vivo PET/MRI with ^{68}Ga-FAPI-04 (day 7 after MI). ^{18}F-FDG image was used to identify areas of infarcted myocardium (arrow), where increased uptake of ^{68}Ga-FAPI-04 was apparent (arrowhead). ^{68}Ga-FAPI-04 exhibited elevated uptake in postsurgical scar (asterisk). Dashed line separates ^{68}Ga-FAPI-04 uptake in myocardium from surgical wound. High-resolution MR and PET/MR data confirmed infarcted area, where ^{68}Ga-FAPI-04 uptake was increased.

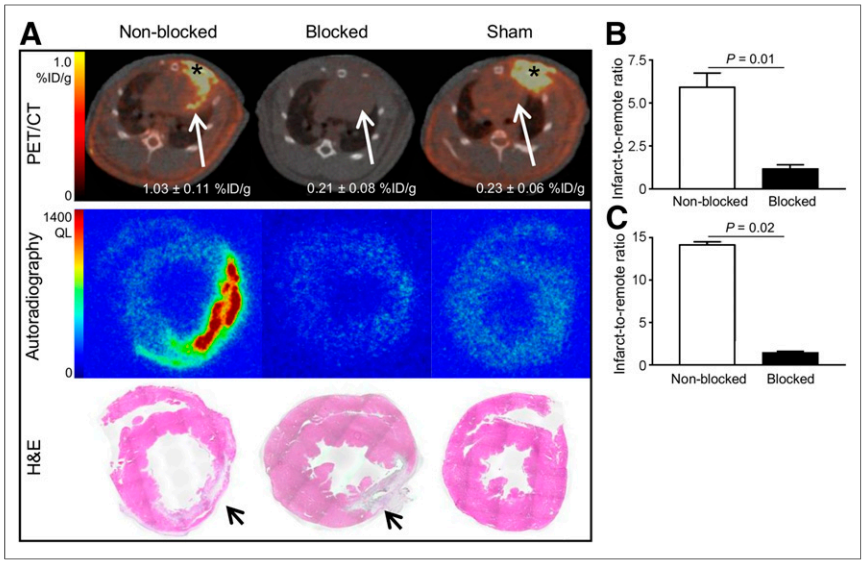

FIGURE 5. Binding specificity test. (A) PET/CT axial views, autoradiographs, and corresponding H&E stainings of 10-μm cross-sections prepared from MI nonblocked, blocked, and sham-operated rats. Autoradiographs and H&E stainings from nonblocked hearts show increased ^{68}Ga-FAPI-04 uptake in infarcted area at 7 d after MI, whereas uptake is negligible after sham operation or injection of nonlabeled FAPI-04 (blocked). Infarcted areas in H&E stainings are identified with arrows. (B) PET image–derived infarct-to-noninfarct uptake ratio (derived from 6 nonblocked and 3 blocked rat hearts subjected to coronary ligation). (C) Autoradiography image–derived infarct-to-noninfarct uptake ratio (derived from 3 nonblocked and 3 blocked MI hearts). QL = quantum level.

In the periinfarcted connective tissue, most FAP$^+$ cells strongly expressed prolyl-4-hydroxylase β whereas fewer FAP$^+$ cells expressed α-smooth muscle actin (Fig. 7D), indicating massive infiltration of FAP$^+$ prolyl-4-hydroxylase β–positive proto-myofibroblasts in the infarct border zone. These data were consistent with previously published data on FAP expression after MI (*8*). Coexpression analyses of vimentin with FAP in liver, lung, and skin demonstrated FAP expression in dermal vimentin-positive fibroblasts only (Supplemental Fig. 3), confirming the presence of activated fibroblasts in skin as evidenced by others (*11*).

DISCUSSION

The present study demonstrated the feasibility of imaging activated fibroblasts after MI using PET and the radiolabeled FAPI ^{68}Ga-FAPI-04. Fibroblast activity in the infarcted myocardium was imaged with PET/CT, with high contrast and minimal uptake in normal myocardium (infarct-to-noninfarct uptake ratio was 6 ± 2 at 6 d after MI) or other organs such as the liver (infarct-to-liver uptake ratio was 11 ± 3 at 6 d after MI). The specificity of the PET signal was confirmed by blocking with nonlabeled FAPI-04 and immunofluorescence staining studies corroborating high expression of FAP by activated fibroblasts. Furthermore, the study showed the feasibility of imaging the time course of fibroblast activation after MI. Peak activity was observed 6 d after coronary ligation and decreased rapidly to the background level by 2 wk after infarction. The signal from ^{68}Ga-FAPI-04 is therefore fundamentally different from contrast enhancement on MRI, which persists for months in the myocardium after infarction. Thus, ^{68}Ga-FAPI-04 shows fibroblast activation and fibrosis formation whereas MRI visualizes the presence of fibrous tissue independent of the activation state of the fibroblasts.

Identification of drugs that selectively inhibit fibroblast activation and transdifferentiation to the ECM-secreting myofibroblast cell state represents an attractive approach to the treatment of fibrosis-related diseases, which include not only MI but also other common diseases such as liver cirrhosis or pulmonary fibrosis (*12*). Antifibrotic treatments inhibiting the pathways responsible for interconversion of quiescent fibroblasts to activated and profibrotic myofibroblasts have shown promise for improving left ventricular function in preclinical studies (*13–15*). However, translation of experimental findings into human patients has been rather limited. One reason is the lack of tools to noninvasively monitor fibroblast activation in patients. Specifically, the favorable roles of myofibroblasts in early infarct healing and the detrimental effects of a prolonged increase in reactive fibrosis require cautious timing for safe and effective antifibrotic treatments. It is therefore conceivable that a diagnostic strategy targeted at detecting active myofibroblasts would allow for a better understanding of their temporospatial presence in the injured myocardium, better estimation of the likelihood of postinfarction heart failure evolution, and better assessment of the efficacy of antifibrosis therapies.

Expansion of fibrosis in areas remote from the infarction, known as reactive fibrosis, is believed to be an important mechanism for the development of heart failure (*3*). In the present study, we did not observe increased uptake of ^{68}Ga-FAPI-04 in the remote uninjured myocardium. However, the experiments were performed on healthy rats that did not show signs of heart failure during the relatively short follow-up period. Future studies on animals with risk factors for the development of post-MI heart failure, such as diabetes (*16*) or hyperlipidemia (*17*), are required to assess the ability of ^{68}Ga-FAPI-04 to monitor fibrosis formation in areas remote from the injured myocardium.

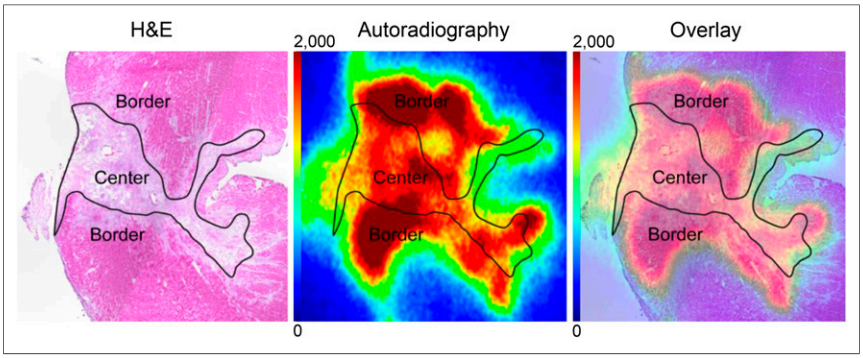

FIGURE 6. Ex vivo evaluation of ^{68}Ga-FAPI-04 uptake in infarct at 7 d after MI. Representative autoradiograph and corresponding H&E staining from rat heart show elevated and heterogeneous uptake of ^{68}Ga-FAPI-04 in infarct border compared with infarct center.

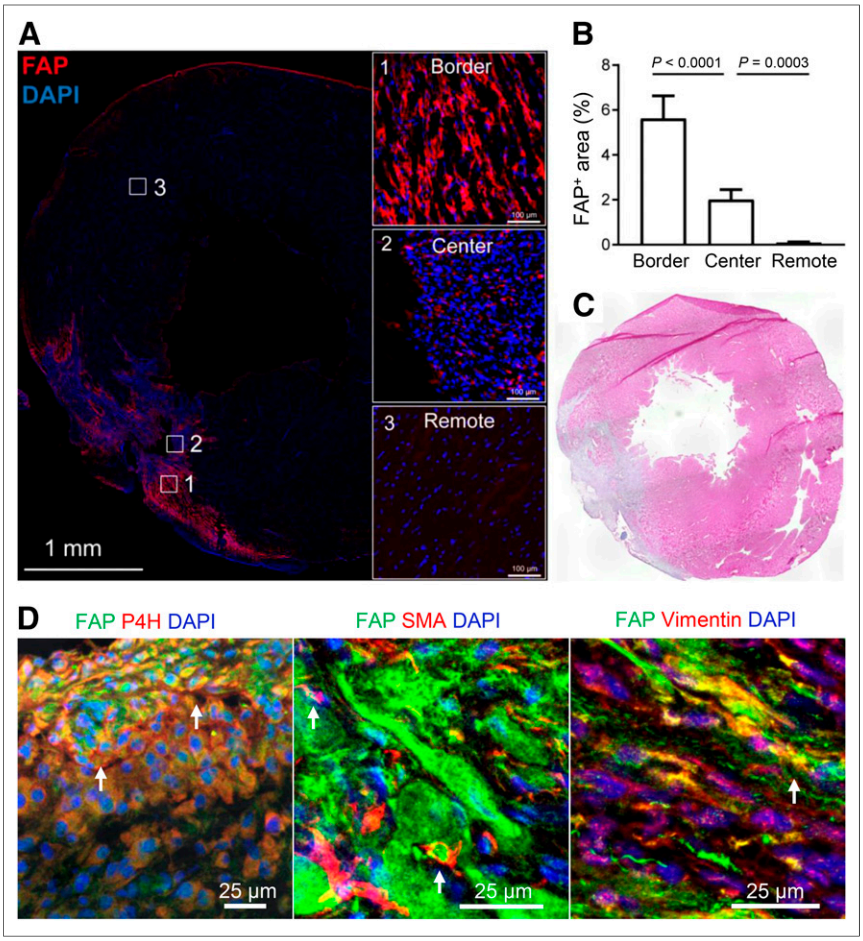

FIGURE 7. (A) Tile scan of entire infarcted heart section showing location of FAP^+ fibroblasts. Insets 1, 2, and 3 show higher magnification from infarct border, infarct center, and noninfarcted remote myocardium, respectively. (B) Enumeration of FAP^+ fibroblast density in MI hearts ($n = 3$) showing higher FAP^+ fibroblast percentage in border zone than in infarct center or remote zone. (C) H&E-stained parallel section. (D) Photomicrographs of FAP, prolyl-4-hydroxylase β (P4H), α-smooth muscle actin, and vimentin-stained infiltrated fibroblasts in periinfarct border zone. Abundant colocalization of FAP, prolyl-4-hydroxylase β, and vimentin shows that accumulated fibroblasts are activated phenotypes, whereas small portion have differentiated into α-smooth muscle actin–positive mature myofibroblasts.

Several candidate biologic processes have been targeted for molecular imaging of cardiac fibrosis, and a variety of ECM components have been tested to this aim (*18*). However, fibrosis is the consequence or endpoint of the fibroblast activation. Once fibrosis has developed, reversal of the deposition of collagen and other proteins in the ECM will generally prove challenging. In contrast, evaluation of fibroblast activation provides indirect evidence of the rate of fibrogenesis or collagen deposition and hence may identify a time window during which fibrosis can still be prevented and the disease course altered.

Upregulated expression of $\alpha_v\beta_3$ in activated fibroblasts has been reported in vitro and in vivo (*18,19*). In some proof-of-concept studies, an arginine-glycine-aspartate imaging peptide has been used to identify proliferating myofibroblasts in postinfarct animal models (*20,21*) and in patients (*22*). However, preclinical and clinical studies documented that $\alpha_v\beta_3$ integrin is expressed not only by activated cardiac myofibroblasts but also by macrophages (*23*) and within endothelial cells of the microvasculature (*24–26*). Therefore, even though $\alpha_v\beta_3$ expression may hold promise as a combined marker of post-MI healing activity (fibroblast activation, inflammation, and angiogenesis), it is not exclusively specific for activated fibroblasts (*6*).

The expression of FAP in myocardial fibroblast subsets was first demonstrated by Tillmanns et al. in frozen sections from rat hearts subjected to permanent ligation of the left anterior descending coronary artery and in paraffin-embedded formalin-fixed tissue samples obtained from the left ventricular apex of MI patients (*8*). It was clearly shown that FAP^+ cells were indeed activated fibroblasts, predominantly protomyofibroblasts, as evidenced by coexpression of FAP with prolyl-4-hydroxylase β, α-smooth muscle actin, and vimentin in rat hearts and with Thy-1 in human hearts (*8*). The researchers then concluded that FAP expression identifies collagen-synthesizing activated, but not resting, fibroblasts. Therefore, imaging of FAP expression provides unique opportunities to study fibroblast activity in the injured myocardium.

On the basis of a small-molecule enzyme inhibitor with high affinity to FAP (*27*), a series of 15 novel FAPI conjugates (FAPI-01 to FAPI-15) was developed by several approaches toward chemical modification (*9,10*). Among other quinolone-based radiopharmaceuticals, FAPI-04 showed improved pharmacokinetic properties regarding target accumulation and retention time (*10*). A comprehensive preclinical evaluation of the tracer led to clinical translation of FAPI-04 for diagnosis and therapy of metastasized cancer in patients (*10*). These initial patient studies showed high uptake of ^{68}Ga-FAPI-04 by several malignancies and only very low uptake by lung, liver, and kidneys. Therefore, we expect that imaging of fibroblast activation after MI will also be feasible in humans using ^{68}Ga-FAPI-04.

We realize that there were limitations to our initial evaluation of FAP imaging of myocardial fibroblasts. First, we imaged the regional presence of activated fibroblasts in the infarcts only after permanent coronary artery occlusion and observed that ^{68}Ga-FAPI-04 accumulated predominantly in the border region. This tracer uptake pattern in the infarct area may be partially attributed to inadequate delivery of radiotracer to the infarct area due to no reflow or poor collateral flow to the infarct central region. Future studies are required to assess ^{68}Ga-FAPI-04 uptake after myocardial infarction in ischemia–reperfusion models. These studies are required to assess if ^{68}Ga-FAPI-04 can image the effect of coronary interventions on the extent of fibroblast activation. However, the model of permanent ligation of the left anterior descending coronary artery used in our study is likewise clinically relevant in that it allows the study of fibroblast activation after MI in the absence of the potentially confounding effects of reperfusion (*28*). Additionally, the potential of ^{68}Ga-FAPI-04 for imaging diffuse fibrosis needs to be evaluated in proper animal models, such as a pressure-overload–induced disease model. These studies are required

to determine how sensitively ^{68}Ga-FAPI-04 can detect myofibroblasts—that is, what density of myofibroblasts is required for a quantifiable signal. However, the very strong in vivo signal obtained after MI (1.0 ± 0.2 %ID/g, day 6 after MI) in the present study, as well as the very low uptake in noninfarcted myocardium (0.2 ± 0.1 %ID/g, day 6 after MI) and neighboring normal organs, suggests that more subtle forms of fibroblast activation will also be detectable by ^{68}Ga-FAPI-04 PET/CT. Finally, because of the presence of high ^{68}Ga-FAPI-04 uptake in the surgical wound region near the infarcts, it was not possible to quantify in vivo PET signal from the infarcts. To avoid the surgical trauma of thoracotomy in open-chest models of coronary ligation and to provide temporal information on changes in FAP expression after MI in a noninvasive and quantitative mode, closed-chest catheter-based models of MI are proposed for future studies.

CONCLUSION

Activation of fibroblasts was imaged noninvasively with high contrast using PET and the FAPI ^{68}Ga-FAPI-04. We expect that the ability to study activated fibroblasts noninvasively and repetitively will provide new insights into ventricular remodeling after MI and possibly also in other cardiac pathologic conditions that are associated with activation of fibroblasts, such as hypertension and ischemic, dilated, and hypertrophic cardiomyopathies (*15*). Further studies of the feasibility of imaging fibroblast activation with ^{68}Ga-FAPI-04 PET/CT in various settings are warranted.

DISCLOSURE

This research was financially supported by Deutsches Zentrum für Herz-Kreislaufforschung (DZHK). Andreas Habenicht and Sarajo Mohanta were supported by Deutsche Forschungsgemeinschaft (DFG): HA 1083/15-4 (Andreas Habenicht) and MO 3054/1-1 (Sarajo Mohanta). No other potential conflict of interest relevant to this article was reported.

ACKNOWLEDGMENTS

We thank Sybille Reder and Markus Mittelhäuser for technical assistance with the PET/CT scans.

KEY POINTS

QUESTION: Is it feasible to dynamically monitor cardiac fibroblast activation after MI with ^{68}Ga-FAPI-04 PET?

PERTINENT FINDINGS: The temporospatial presence of activated fibroblasts in the infarcted myocardium was imaged using ^{68}Ga-FAPI-04 PET/CT. The local accumulation of ^{68}Ga-FAPI-04 peaked on day 6 after MI, mainly in the infarct border zone.

IMPLICATIONS FOR PATIENT CARE: Noninvasive detection of active fibroblasts would help clinicians assess the likelihood of evolution of heart failure after MI and monitor the efficacy of antifibrosis therapies.

REFERENCES

1. Mendis S, Puska P, Norrving B. *Global Atlas on Cardiovascular Disease Prevention and Control.* Geneva, Switzerland: World Health Organization; 2011: 3–18.
2. Bahit MC, Kochar A, Granger CB. Post-myocardial infarction heart failure. *JACC Heart Fail.* 2018;6:179–186.
3. Talman V, Ruskoaho H. Cardiac fibrosis in myocardial infarction: from repair and remodelling to regeneration. *Cell Tissue Res.* 2016;365:563–581.
4. van den Borne SW, Diez J, Blankesteijn WM, Verjans J, Hofstra L, Narula J. Myocardial remodelling after infarction: the role of myofibroblasts. *Nat Rev Cardiol.* 2010;7:30–37.
5. Rog-Zielinska EA, Norris RA, Kohl P, Markwald R. The living scar: cardiac fibroblasts and the injured heart. *Trends Mol Med.* 2016;22:99–114.
6. de Haas HJ, van den Borne SW, Boersma HH, Slart RH, Fuster V, Narula J. Evolving role of molecular imaging for new understanding: targeting myofibroblasts to predict remodeling. *Ann N Y Acad Sci.* 2012;1254:33–41.
7. Garin-Chesa P, Old LJ, Rettig WJ. Cell surface glycoprotein of reactive stromal fibroblasts as a potential antibody target in human epithelial cancers. *Proc Natl Acad Sci USA.* 1990;87:7235–7239.
8. Tillmanns J, Hoffmann D, Habbaba Y, et al. Fibroblast activation protein alpha expression identifies activated fibroblasts after myocardial infarction. *J Mol Cell Cardiol.* 2015;87:194–203.
9. Loktev A, Lindner T, Mier W, et al. A tumor-imaging method targeting cancer-associated fibroblasts. *J Nucl Med.* 2018;59:1423–1429.
10. Lindner T, Loktev A, Altmann A, et al. Development of quinoline-based theranostic ligands for the targeting of fibroblast activation protein. *J Nucl Med.* 2018;59:1415–1422.
11. Janson DG, Saintigny G, van Adrichem A, Mahé C, El Ghalbzouri A. Different gene expression patterns in human papillary and reticular fibroblasts. *J Invest Dermatol.* 2012;132:2565–2572.
12. Bollong MJ, Yang B, Vergani N, et al. Small molecule-mediated inhibition of myofibroblast transdifferentiation for the treatment of fibrosis. *Proc Natl Acad Sci USA.* 2017;114:4679–4684.
13. Thum T, Gross C, Fiedler J, et al. MicroRNA-21 contributes to myocardial disease by stimulating MAP kinase signalling in fibroblasts. *Nature.* 2008;456: 980–984.
14. Bradley JM, Spaletra P, Li Z, et al. A novel fibroblast activation inhibitor attenuates left ventricular remodeling and preserves cardiac function in heart failure. *Am J Physiol Heart Circ Physiol.* 2018;315:H563–H570.
15. Creemers EE, Pinto YM. Molecular mechanisms that control interstitial fibrosis in the pressure-overloaded heart. *Cardiovasc Res.* 2011;89:265–272.
16. Greer JJ, Ware DP, Lefer DJ. Myocardial infarction and heart failure in the db/db diabetic mouse. *Am J Physiol Heart Circ Physiol.* 2006;290:H146–H153.
17. Maczewski M, Maczewska J. Hypercholesterolemia exacerbates ventricular remodelling in the rat model of myocardial infarction. *J Card Fail.* 2006;12:399–405.
18. de Haas HJ, Arbustini E, Fuster V, Kramer CM, Narula J. Molecular imaging of the cardiac extracellular matrix. *Circ Res.* 2014;114:903–915.
19. Asano Y, Ihn H, Yamane K, Jinnin M, Mimura Y, Tamaki K. Increased expression of integrin $\alpha_v\beta_3$ contributes to the establishment of autocrine TGF-β signaling in scleroderma fibroblasts. *J Immunol.* 2005;175:7708–7718.
20. van den Borne SW, Isobe S, Verjans JW, et al. Molecular imaging of interstitial alterations in remodeling myocardium after myocardial infarction. *J Am Coll Cardiol.* 2008;52:2017–2028.
21. van den Borne SW, Isobe S, Zandbergen HR, et al. Molecular imaging for efficacy of pharmacologic intervention in myocardial remodeling. *JACC Cardiovasc Imaging.* 2009;2:187–198.
22. Verjans J, Wolters S, Laufer W, et al. Early molecular imaging of interstitial changes in patients after myocardial infarction: comparison with delayed contrast-enhanced magnetic resonance imaging. *J Nucl Cardiol.* 2010;17:1065–1072.
23. Antonov AS, Kolodgie FD, Munn DH, Gerrity RG. Regulation of macrophage foam cell formation by αVβ3 integrin: potential role in human atherosclerosis. *Am J Pathol.* 2004;165:247–258.
24. Meoli DF, Sadeghi MM, Krassilnikova S, et al. Noninvasive imaging of myocardial angiogenesis following experimental myocardial infarction. *J Clin Invest.* 2004;113:1684–1691.
25. Brooks PC, Clark R, Cheresh D. Requirements of vascular integrin alpha v beta 3 for angiogenesis. *Science.* 1994;264:569–571.
26. Jenkins WS, Vesey AT, Stirrat C, et al. Cardiac $\alpha_v\beta_3$ integrin expression following acute myocardial infarction in humans. *Heart.* 2017;103:607–615.
27. Jansen K, Heirbaut L, Cheng JD, et al. Selective inhibitors of fibroblast activation protein (FAP) with a (4-quinolinoyl)-glycyl-2-cyanopyrrolidine scaffold. *ACS Med Chem Lett.* 2013;4:491–496.
28. Hausenloy DJ, Yellon DM. Myocardial ischemia-reperfusion injury: a neglected therapeutic target. *J Clin Invest.* 2013;123:92–100.